

Ruđer Bošković Institute, Center for marine and environmental research, Zagreb, Croatia

ERA-40 aided assessment of the atmospheric influence on satellite
retrieval of the Adriatic Sea surface temperature

Igor Tomažić and Milivoj Kuzmić

With 6 figures

Summary

The aim of this work has been assessment of regional atmospheric influence on satellite derivation of the Adriatic Sea surface temperature (SST). To that end the ECMWF ERA-40 reanalysis dataset has been employed to provide the temperature and humidity profiles and surface data, while the RTTOV 8.7 radiative transfer model was used to calculate the top of atmosphere brightness temperatures for the AVHRR channels. Ten ERA-40 grid points over the Adriatic Sea were used in the analysis, providing 29590, 00 UTC and 12 UTC, clear-sky profiles.

Climatological analysis of the ERA-40 profiles demonstrated a distinct seasonal variability over the Adriatic. Seasonality noted in the temperature and specific humidity profiles also evinced in the atmospheric transmittance, thermal channels temperature deficit, and derived γ and ρ parameters. A multivariate analysis was applied to relate the simulated top of the atmosphere (TOA) brightness temperatures (BT) to the Adriatic SSTs, in order to generate exploratory sets of SST retrieval coefficients. All 10 derived coefficient sets exhibited smaller noise amplification factor than the global counterpart. A test comparison of satellite-derived SST with an eleven-month in situ SST series showed that locally derived coefficients provide smaller scatter (improved precision), and bias that requires empirical adjustment before operational use. Almost identical SST residual and metrics was obtained with seasonally adjusted “classical” split-window coefficients and with coefficients explicitly accommodating water vapour dependence. The comparison to data has reinforced the notion that the over-the-Adriatic atmosphere may exhibit variability which globally adjusted correction can not fully accommodate.

1. Introduction

Sea surface temperature (SST) is an important variable in climate monitoring and weather forecasting as well as in many other atmospheric or oceanographic empirical and modelling studies. Satellite SST data have been collected globally for almost three decades, enjoying in the process all the advantages, but also suffering the drawbacks of remote sensing. An important problem is the atmospheric interference with the surface thermal radiation. When surface thermal signal is passing through the atmosphere a fraction of it is absorbed by atmospheric constituents (e.g. water vapour, aerosols, or ozone) and re-emitted at different wavelengths. Thus the information about the atmospheric along-path concentrations of aerosols, ozone and water vapour in particular is very important (Minnett, 1990; Tanre et al., 1992). The net atmospheric effect is to reduce thermal radiation reaching the sensor, and consequently to lower the brightness temperature registered there. If one is to derive satellite SST properly, a correction of measured radiance is needed to account for the mentioned effects. The fact that these influences are wavelength dependent and spatially and temporally variable further aggravates the problem.

The atmosphere exhibits spectral windows where the sea surface thermal radiation peaks, atmospheric attenuation is reduced and reflected solar radiation is low. The radiative transfer of the surface signal through the atmosphere can be defined as:

$$L_{\text{toa}}(\nu, \theta) = \epsilon_s(\nu, \theta) B(T_s) \tau_s(\nu, \theta) + L_{\text{ua}}(\nu, \theta) + L_{\text{rda}}(\nu, \theta) + L_{\text{rs}}(\nu, \theta) \quad (1)$$

where L_{toa} is radiance emerging at the top of the atmosphere (TOA), ν is frequency, θ is the satellite zenith angle, and ϵ_s , T_s , and τ_s are surface emissivity, temperature and transmittance, respectively. The second, third and fourth term stand for the upwelling atmospheric thermal radiation, reflected downwelling atmospheric radiation, and surface-reflected solar radiance, respectively; B is the Planck function. If the atmospheric effects could be specified and the

surface effects could be well characterized, the equation (1) would render the surface temperature. However, direct inversion from the radiative transfer equation is a tall order, so approximations are necessary if one is to obtain solutions, operational ones in particular.

Various simplified approaches have been proposed to account for atmospheric attenuation of the surface-leaving infrared radiance, usually ignoring the effect of non-unity surface emissivity. Since the work of Anding and Kauth (1970) the difference measurements in two separate infrared channels (differential absorption) is commonly used to estimate the amount of required atmospheric correction. In such a framework it is necessary to assume equal average atmospheric temperature in two spectral windows/channels and to have independent measurement of the brightness temperature in each of them (McMillin, 1975). The setup then leads to algorithms of the form:

$$T_s = A0(\epsilon, wv, L_{rda}, \theta) + A1(\epsilon, wv, L_{rda}, \theta) \cdot T_1 + A2(\epsilon, wv, L_{rda}, \theta) \cdot T_2 \quad (2)$$

often cast in somewhat modified form:

$$T_s = a_0 + a_1 \cdot T_1 + a_2 \cdot [T_1 - T_2] \quad (3)$$

where T_1 and T_2 are sensor's channel brightness temperatures (BT), and a_i are empirical coefficients, assumed constant; wv stands for water vapour. Water vapour is the most important absorber in the 10-13 μm window (e.g. Anding and Kauth, 1970). Absorption by water vapour yields temperature deficit which, if not corrected for, creates an error in the SST estimates, larger for off-nadir satellite viewing angles. The coefficients in a SST algorithm can be derived either by regression of satellite, or radiative-transfer model (RTM) derived BTs against *in situ* temperature data. The former approach has been practiced in numerous studies using the Advanced Very High Resolution Radiometer (AVHRR) retrievals (e.g. Strong and McClain, 1984), whereas the latter characterizes the processing of the Along Track Scanning Radiometer (ATSR) data (e.g. Zavody et al, 1995).

Although the AVHRR-related algorithms have undergone numerous changes their consistent performance over global range of atmospheric conditions still remains a challenge. A major cause of poor validation statistics appears to be (over)simplifications of equation (1) in operational algorithms and misrepresentation of regional atmospheric spatial and temporal variability. An approach that appears to partly ameliorate the problem, producing consistent results on global scale (accuracy of $0.02 \pm 0.5^{\circ}\text{C}$), is estimation of the algorithm coefficients on monthly basis (Kilpatrick et al., 2001), distinguishing two (wet and dry) atmospheric regimes. Acknowledging temporal variability still leaves open the question of regional suitability of global solutions. Regional and/or time-limited applications need not take into account the full range of atmospheric variability, but should include regional and/or seasonal dependence (Minnett, 1990). Exploring the errors associated with the SST retrievals from the Indian Ocean Sheno (1999) obtained considerably improved validation statistics with regionally optimized SST algorithm coefficients. Eugenio et al. (2005) used a subset of the Pathfinder matchup database to derive SST algorithm coefficients optimized for the Canary Islands – Azores – Gibraltar region. Requesting spatial and temporal coincidence of ± 10 km and ± 30 min respectively the authors devised a new algorithm with considerably improved statistics (mean error of 0.0748°C , RMS error of 0.58°C). Focusing on just the Canary Island zone, Arbelo et al. (2000) demonstrated inadequate performance of the global SST algorithm (derived for 6 standard atmospheres). Compared to their regional algorithm (derived for the local atmosphere characterized with thirty radiosonde temperature and humidity profiles) global algorithm generated mean error difference of $+0.3$ K, and about twice as large RMS difference. However, a recent study (Merchant et al., 2006) warns that although sub-optimal choice of retrieval coefficients degrades an estimate, some errors are intrinsic consequence of the retrieval equation form, a simplified example of which is the equation (1).

In this paper we study the atmospheric influence on the SST derivation from satellite data over the Adriatic Sea. In addressing the problem our goal is not to derive a new operational algorithm, but rather to assess the extent of the local atmospheric influence on such a product. More specifically, we have firstly addressed the seasonal temperature and humidity variability of the atmosphere over the Adriatic, followed by deriving test SST retrieval coefficients reflecting that variability, and then gauging their impact on the Adriatic SST estimates. The atmospheric variability over the Adriatic Sea was explored using the clear sky temperature and humidity profiles from the European Centre for Medium-Range Weather Forecast (ECMWF) ERA-40 re-analysis (Uppala et al., 2005) . An accurate fast radiative transfer model, RTTOV 8.7 - Saunders and Brunel (2005), was then used to simulate brightness temperature in AVHRR channels (4 and 5) using atmospheric profiles and SST values obtained from ERA-40.

The rest of the paper is organised as follows. The data obtained from the ERA-40 re-analysis are discussed in the second section. In the third section we briefly present the RTTOV model and in the fourth section discuss results of the analysis. Conclusions are given in the last section.

2. Data

The dataset employed in this study is an Adriatic subset of the ECMWF ERA-40 reanalysis data (Uppala et al., 2005). The ERA-40 reanalysis covers the period from September 1957 to August 2002. The reanalysis was done with T159 spherical-harmonic representation of upper air fields, and on reduced Gaussian grid N80 providing data on the corresponding regular latitude/longitude resolution of $1.125^{\circ} \times 1.125^{\circ}$ at 60 vertical model-pressure levels between the surface and the 0.1 hPa level. ERA-40 data are available at 00:00, 06:00, 12:00 and 18:00 UTC over a 45-year period. The climatological analysis and the RT model simulations were done using the ERA-40 temperature, specific humidity as well as

integrated (total column water vapour) and surface data (2m air temperature, sea-level pressure, and SST). From the global model grid, only ten grid points over the Adriatic Sea (“wet” as defined by the land-sea mask) were extracted. The positions of the selected Adriatic grid points are shown in Figure 1. We adopted the convention that the points north of the 43° N latitude belong to the northern Adriatic, those south of 42° N to the southern, and those between the two latitudes to the central Adriatic.

One of the ERA-40 variables is the skin temperature, a post-processed variable close to what the model atmosphere “feels” as the sea temperature boundary condition (A. Beljaars, personal communication). More precisely, the open water temperature (SST in our case) is just one tile in an eight-tile scheme (TESSEL - Tiled ECMWF Scheme for Surface Exchanges over Land). The SST used in the open waters tile, and kept constant during the integration, is from July 2000 onward based on the NCEP daily analyses based on ship, buoy and satellite observations (Persson and Grazzini, 2007). Other sources and/or different schemes were used prior to the year 2000, but common to all is the bulk nature of this variable. Therefore, both the skin effect and diurnal cycle were ignored (constant SST value used during an integration period) in the ECMWF simulation runs (Beljaars, 1998). Furthermore, any sub-area retrieval from the Meteorological Archive and Retrieval System (MARS) by definition invokes interpolation of the archived reduced Gaussian grid values further affecting the extracted SST. Nevertheless the use of the SST variable in the radiative transfer modelling together with related ERA40 temperature and humidity profiles is deemed justified in providing TOA BT estimates, bearing in mind that on any given hour ERA40 SST does not exactly correspond with actual surface condition.

Since SST retrieval schemes use clear pixels, only clear sky profiles from ERA-40 were used in the study. Altogether, 29590 cloudless profiles of temperature, humidity and ozone and related surface parameters were extracted over the Adriatic (only the 00 UTC (nighttime)

and 12 UTC (daytime) values). The profiles exhibit seasonal and geographical distribution as summarized in Table 1. The smallest numbers of profiles have been obtained for the northern Adriatic autumn at 00 UTC (196), whereas the largest subset (5088) was collected for the southern Adriatic summer at 00 UTC. The ERA-40 60-level profiles were further interpolated to 43 RTTOV pressure levels using a spline-based program (Chevallier, 2001).

The SST validation data were collected during the period February 2 - December 26 2004 at the INAgip platform Ivana-A in the northern Adriatic (44.745°N, 13.294°E - Figure 1). The Aanderaa Temperature Profile Recorder TR7 (absolute accuracy $\pm 0.05^\circ\text{C}$) was used to collect the data, with the recording depth and interval set to 1 m and 20 min, respectively. These data were paired with the related temperatures registered with the AVHRR/3 instrument aboard NOAA 16 satellite to create a matchup database. Satellite data were received at the local HRPT receiving station (Quorum Communications) and converted to the level 2 format. AAPP package (Klaes, 1997) was used to convert data from the level 0 to level 1b format, and custom build application was employed to convert the data from the level 1b to level 2 format. Additional navigation corrections were performed with the ANA3 application (Bordes et al., 1992; Brunel and Marsouin, 2000). For the time period considered there were 576 daytime and 576 night time scenes. The pairing was performed observing relatively tight spatial and temporal constraints. The included satellite pixels have been located within the pixel-size distance from the Ivana-A platform location, and registered within 15 minutes of the measurement at the Ivana-A platform. These criteria provided 578 daytime and 542 nighttime matchup records. Prior to the pairing, all scenes were cloudmasked using a suit of spectral tests (separately for day and night) based on visible and thermal channels data and related threshold values optimized for the Adriatic (Tomažić, 2006). The application of the cloudmasking algorithm, restriction for too large satellite zenith angle, and additional requirement on brightness temperatures (standard deviation in a 3x3 pixel window centred on

Ivana-A station less than 0.12°C , cf. Eugenio et al., 2005) further reduced the number of useful matchup records. The final score was 102 daytime and 92 nighttime pairs.

3. Radiative transfer model

RT-model simulation of the upwelling thermal radiation requires modelling of radiation interaction with the atmospheric constituents. That can be computationally demanding when performed with line-by-line models, but simplified fast RTMs exist, providing viable alternative. One such model, the RTTOV in its version 8.7, has been used in the present work (Saunders and Brunel, 2005). The original code has undergone several modifications, most recently by the EUMETSAT numerical weather prediction (NWP) Satellite Application Facility (SAF). It follows a line of improvements (Eyre, 1991; Rayner, 1995), originating from the work of Eyre and Woolf (1988), itself building on the work of McMillin and Fleming (1976). Given atmospheric profile of temperature and humidity together with surface temperature and pressure, as well as satellite zenith angle, the model in forward mode computes the TOA radiances in each of the channels of the sensor being simulated. Atmospheric profiles of ozone and carbon dioxide, and surface emissivity can be provided optionally, but these options were not used in the present study.

The RTTOV model can simulate both the clear sky and cloudy radiances using an approximate atmospheric radiative transfer equation. The top of the atmosphere clear sky upwelling radiance $L^{\text{clr}}(\nu, \theta)$ (pertinent to our study), at the frequency ν , zenith angle θ , and neglecting scattering effects (Saunders and Brunel, 2005) reads:

$$L^{\text{clr}}(\nu, \theta) = \tau_s(\nu, \theta) \varepsilon_s(\nu, \theta) B(\nu, T_s) + \int_{\tau_s}^1 B(\nu, T) d\tau + (1 - \varepsilon_s(\nu, \theta)) \tau_s^2(\nu, \theta) \int_{\tau_s}^1 \frac{B(\nu, T)}{\tau^2} d\tau \quad (4)$$

where the terms on the right correspond to the terms in (1), ignoring the reflected solar radiation. T is atmospheric temperature.

In the RTTOV versions prior to number six, blackness of all surface types was default (emissivity equal to one). In the RTTOV 6 channel average sea surface emissivity default was introduced, calculated after Masuda et al. (1988), allowing for zenith angle dependence while keeping zero wind speed (Sherlock, 1999). The same emissivity model is in effect in the RTTOV version used in present study. Merchant and LeBorgne (2004) examined accuracy and precision of four different RTMs (including the RTTOV-7). They found the models not absolutely accurate enough to specify the offset coefficient to desired accuracy of 0.1K. Within the scope of performed validation studies the RTTOV-8 has shown performance similar to RTTOV-7 (Saunders and Contributors, 2005).

4. Results and Discussion

Addressing the local atmospheric influence on satellite-derived Adriatic Sea surface temperature we will first analyse in this section the temperature and humidity variability over the Adriatic Sea as derived from ERA-40 data, and then assess the influence of that variability on the SST retrieval coefficients. Changeable features of the atmospheric humidity exert great influence on the earth-emitted long-wave radiation, but specific quantitative studies of vertical distribution of humidity in the Mediterranean area in general, and over the Adriatic Sea in particular, appear to be nonexistent. We have therefore taken as the reference situations the average conditions embodied in the mid-latitude profiles.

4.1 Seasonal atmospheric variability

In order to examine the extent of local atmospheric variability separate analyses of the ERA-40 temperature and humidity profiles were performed for different seasons. Preliminary

analysis of intra-Adriatic geographic variability did not produce enough variability to warrant further consideration. The result for temperature is presented in Figure 2. The comparison of ERA-40 derived seasonal temperature profiles with respective mean profile for the Adriatic exhibits marked variability (Figure 2a-d). Seasonal temperature variations can be seen to the pressure levels in the higher troposphere and lower stratosphere (to the pressure level of 194 hPa), and are the most significant at the lowest pressure levels. More significant difference in mean and standard deviation (horizontal bars) can be seen in the winter (Q1) and summer (Q3) period. We further compared the ERA-40 Adriatic seasonal average winter and summer profiles to the respective mid-latitude data (Figure 2e). Comparison suggests that the ERA-40 derived winter lower troposphere is warmer than the mid-latitude average by as much as 10 K. The summer profile is more similar to its mid-latitude counterpart, diverging from it toward higher values in the lower troposphere. The Adriatic ERA40 derived multi-annual average turns out somewhat warmer than the US Standard Atmosphere, throughout the troposphere, and in its middle part in particular (Figure 2f).

Monthly averaged Adriatic 2m air temperatures calculated from the ERA-40 dataset exhibit a clear seasonal cycle. In Figure 2g those values for two model points (R and K in Figure 1) are compared to related in situ climatology from the two nearest coastal stations (Rovinj and Korčula – see Figure 1). The field data (http://www.hhi.hr/archi_pelago/naslov/e_temp.htm) were available only for the 1981-1995 period so the ERA40 series was shortened accordingly. One notes a close correspondence between the measured and modelled data, with the ERA40 values being persistently somewhat higher than the measured temperatures at the northern (Rovinj) station; the opposite appears to hold at the southern (Korčula) station. In this comparison one has to bear in mind the natures of the ERA40 SST series elaborated in the data section.

The results of the specific humidity analysis are presented in Figure 3. Specific humidity seasonal variations go up to 300 hPa pressure level. Significant differences in the mean and standard deviation (horizontal bars) can be observed in all seasons. The only exception is the spring profile which remains very similar to the annual mean. Again, the most distinct seasonal differences in the mean are observed in winter, and least significant in spring (Figures 3a and 3c). It is worth noting that the winter mean profile in particular is much drier than the annual mean. The seasonal difference may be further appreciated by inspecting the Figure 3e. One may see that the ERA-40 derived winter specific humidity follows relatively closely the mid-latitude average except in the lowermost layers where the Adriatic profile exceeds. Similar difference is observed between the average Adriatic and US Standard Atmosphere (Figure 3f), only the point of disagreement starts higher, close to the 700 hPa level.

The noted variability is also seen in Table 2 where numerical values of seasonal and layer averages of temperature and specific humidity are listed. The first two columns list the average values of the atmospheric temperature above (T_L) and below (T_U) the 850 hPa level. The chosen pressure level conveniently divides the mean vertical distribution of the specific humidity (Minnett, 1986); in the text that follows we will refer to these parts as the upper and lower atmosphere. The next two columns list the respective specific humidity values.

Seasonally, the winter T_L is about 11K lower, and summer T_L some 4 K higher than the annual average. Similarly, winter q_U is about 0.5 gkg^{-1} below, and the summer q_U about 0.2 gkg^{-1} above, the annual average. The lower and upper temperature and humidity annual averages are somewhat larger than the respective US standard atmosphere values. In a study based on a hundred marine radiosonde profiles over the northeastern Atlantic Ocean in July, Minnett (1986) simulated effects of anomalous atmospheric conditions by independently adjusting humidity and temperature profiles. He found that consequences of humidity

anomalies are greater when occurring at greater height (below the 850 hPa level, where the water vapour is colder), whereas temperature anomalies exhibit greater effect at lower height (above the 850 hPa level, where a change of few Kelvin in the water vapour to sea surface temperature difference counts more).

Another view of the noted seasonal changes of the Adriatic atmosphere is presented in Figure 4 where the annual cycle of monthly anomaly of several parameters is plotted. Both the daytime (solid line) and nighttime (dashed line) variability is plotted, exhibiting the same pattern and minor differences in value. Specific humidity anomaly in the upper atmosphere (below 850 hPa) is plotted first (Figure 4a), crossing the 45-year average line between April and May on the way up, and in October on the way down. The temperature anomaly of the lower troposphere (Figure 4b) exhibits the same transition points (late April, and late October), reaching top values in July and August. The standard deviation is lower (2.5 – 3.0 °C) during the period of positive anomaly than during negative (3.5 °C). The total column water vapour (Figure 4c) peaks in August, exhibiting more variability during the warmer part of the year. The temperature difference at the air-sea interface, as registered in the ERA40 database, shows about a month earlier transition to positive values (Figure 4d), and change to negative values in October, as other plotted variables. One should also note that in the peak months of July and August in particular there were twice as many cloud clear data points at 00:00 UTC than at noon (Figure 4e).

As pointed out in the previous paragraphs the atmospheric water vapour is dominant cause of SST signal attenuation. In the split-window framework the differential absorption between AVHRR channels 4 and 5 is used to correct for its adverse effect. A closer look at the total column water vapour (tcwv) and thermal channels' brightness temperatures is taken in Figure 5 where for each month the tcwv is plotted as a function of the $T_4 - T_5$ difference. The tcwv values are taken from the ERA40 database whereas the brightness temperatures

have been calculated using the RT model and assuming zenith angle of zero and NOAA16 spectral response function (SRF). Only daytime result is shown; the nighttime data show differences in detail, but exhibit the same pattern of annual variability. Perhaps predictably, the cluster of data point is the smallest for winter months (December, January) with temperature differences spanning the 0 – 1 °C range, and water vapour content staying below 20 kgm⁻². The cluster attains the largest size in summer (July, August) when differences larger than 2°C are found, and tcwv values can reach the 40 kgm⁻² level. A look at the seasonally averaged temperature deficit in each channel (Table 3) provides a further insight. In both channels the temperature deficit due to the atmospheric absorbers is smallest in winter and largest in summer, with spring and autumn values bridging the extremes. The multi-annual average deficit is larger than -2.5 K in channel 5 where the atmospheric load is greater; the nighttime values systematically exceed the daily counterparts. Also included in the table are two derived parameters. The first is a ratio reflecting both the state of the sea surface and the atmosphere above it. It may be defined as (see e.g. Kleespies and McMillin, 1990):

$$\rho = \varepsilon_5 \tau_5 / \varepsilon_4 \tau_4 \quad (5)$$

where ε and τ are the sea surface emissivity and surface to TOA transmittance, and the subscripts refer to the AVHRR channel 4 and 5 respectively. The parameter relates the changes in channel 4 and channel 5 transmittances (and also the changes in respective brightness temperatures) for a given change in the sea surface temperature. The channel 4 and channel 5 transmittances (not shown) exhibit their highest values in winter, and lowest in summer so the ρ parameter follows the variability pattern with the minimum in summer and the maximum in winter. The other parameter, representing intrinsic differential absorption term, can be expressed as (McMillin, 1975):

$$\gamma = (1 - \tau_4) / (\tau_4 - \tau_5) \quad (6)$$

where τ_4 and τ_5 are, as before, the AVHRR channel 4 and channel 5 transmittances. We list in Table 3 its value derived with the aid of equation (6), using transmittances calculated with the RTTOV model for the AVHRR sensors onboard NOAA16. The γ values we obtained appear to reflect seasonal variations noted in atmospheric temperature and humidity data, exhibiting minor difference among parts of the Adriatic, or between daytime and nighttime. In both cases the values are larger in warmer and smaller in colder part of the year, and always smaller than a typical global value (~ 2.5).

In summary, over-the-Adriatic profiles near-surface values as well as examined RT model-derived parameters evince distinct seasonal variability, of water vapour in particular. Any algorithm devised to estimate the Adriatic SST must accommodate the impact. In the split-window framework the differential absorption term is meant to compensate for the atmospherically caused temperature deficit. In the next section we therefore examine the successfulness of three particular algorithms (one commonly used and two derived in present framework) in providing the needed correction.

4.2 Derivation and assessment of the Adriatic SST coefficients

Two methods (empirical and theoretical) are commonly employed in deriving the SST retrieval coefficients (see e.g. Minnett, 1990). Both rely on regression analysis but differ in sources of the regression pairs. In the empirical approach, as the name suggests, the satellite-derived brightness temperatures are paired with collocated in situ measurements, whereas in the latter approach a radiative transfer model is used to simulate a range of atmospheric conditions, enabling pairing of simulated brightness temperatures with corresponding SST values. One particularly important difference is that the former method provides bulk temperature estimates (usable in comparison with the usual oceanographic measurements) whereas the latter estimates the skin temperature (still not routinely measured in the field).

The AVHRR global coefficients are derived with the empirical method, whereas in this study we used theoretical method, bearing in mind the limitations outlined in the data section. Before reaching the satellite sensor as TOA brightness temperature (T_B), the sea surface temperature (T_s) signal is subject to a) in situ sensor error uncertainty, b) skin/diurnal warming uncertainty, c) atmospheric variability, and d) satellite sensor error uncertainty. In our case, typical a) contribution to the overall uncertainty is ± 0.05 K, that of d) is ± 0.12 K (Trishchenko et al, 2002) but the b) part uncertainty is rather difficult to estimate (although it can cause differences of several K; diurnal excursions exceeding 6K have been observed with an estimated error of 0.3 K, Merchant et al, 2008). The radiometric noise and in situ sensor errors were not explicitly considered in the validation process, but understood as contributors to the SST error residual.

The split-window algorithms commonly account for intervening atmosphere using linear combinations of brightness temperatures in different AVHRR channels, an approach for which McMillin (1975) provides early justification. Studies have shown (e.g. Zhang et al., 2004) that with such an approach globally tuned algorithms may generally have small biases while exhibiting large regional discrepancies, producing regionally either positive or negative biases. Put differently, globally fixed coefficients can produce inaccurate SST estimates (exhibit systematic retrieval error) when local atmospheric conditions differ from the implicit average state, known as the first guess and captured in the regression procedure (Eyre, 1987). Such an error exhibits regional and seasonal variability (O'Carroll et al, 2006).

In order to address possible impact of the noted over-the-Adriatic atmospheric variability on satellite SST estimates, the ERA-40 SSTs and the RTTOV-derived TOA BTs were subjected to a multivariate analysis. The analysis was done for 7 different zenith angles (from 0° to 60°), with the ERA-40 profiles split into daytime and nighttime sets. The following MCSST split window algorithm

$$SST = -a_0 + a_1 T_4 + a_2 (T_4 - T_5) + a_3 (T_4 - T_5) (\sec(\theta_{zen}) - 1) \quad (7a)$$

was used, separately for daytime and nighttime. To address the impact of the tcwv a generic form of algorithm is used, again separately for day and night:

$$SST = -a_0 + a_4 W + a_5 W^2 + a_1 T_4 + a_2 (T_4 - T_5) + a_3 (T_4 - T_5) (\sec(\theta_{zen}) - 1) \quad (7b)$$

In the above algorithms T_4 and T_5 are AVHRR brightness temperatures, θ_{zen} is the satellite zenith angle, and a_0 to a_3 , d or n, are the daytime and nighttime regression coefficients. W is equal to $tcwv/\cos(\theta_{zen})$. Ten coefficient sets (5+5) derived for NOAA16 are listed in Table 4. Four seasonal sets were derived using (7a), and just one annual was produced using the water vapour algorithms (7b). To those two global sets are added for reference. Also listed, next to the a_2 coefficient, is the noise amplification factor (NAF). NAF is defined, following Pearce et al., 1989, as:

$$NAF = \sqrt{(a_1 + a_2)^2 + a_2^2} \quad (8)$$

where a_i are appropriate coefficients from equations (7) reported in Table 4; contribution of off-nadir viewing (a_3) is not considered. It measures the amplification of the noise due to the intrinsic instrumental uncertainty in channel brightness temperature measurements, introduced into the SST estimates with particular set of coefficients. Inspection of the coefficient values readily reveals a pattern in global-Adriatic differences. The values of the a_1 coefficient, which scales the direct contribution of the channel 4 brightness temperature, is very close to one in the global set, as well as in all the Adriatic sets. On the other hand, for all derived sets the a_2 Adriatic values, which control the amount of the applied differential absorption correction, are all about 1.3 or higher, but smaller than 2. One also notes that, in keeping with the results reported in section 4.1, the Adriatic a_2 coefficients suggest larger differential absorption correction (and consequent noise) in spring and summer than in autumn and winter. All Adriatic a_2 values are also smaller than the respective global values, while exhibiting seasonal differences. Very similar variability pattern is observed in the γ parameter (Table 3), which

may be viewed as the "intrinsic a_2 ", calculated with the aid of equation (6) and therefore independent of the regression analysis. The change in a_2 is accompanied with changes in the offset coefficient a_0 and the a_3 coefficient, accounting for the off-nadir paths contribution to the atmospheric correction. It is noteworthy to reiterate that while the Adriatic a_1 values are close to global ones, all Adriatic a_2 values are smaller than 2 while the respective global values are larger. An important consequence of the reduced coefficient values is decreased noise amplification in all Adriatic algorithms. Furthermore, for both daytime and nighttime the autumn and winter algorithms appear less noisy than their spring and summer counterparts.

To probe the extent to which noted variability affects the Adriatic SST estimates we calculated the SST estimates with four different algorithms/coefficient sets and compared the outcome with the SST Ivana-A measurements. The result of the exercise is graphically presented in Figure 6 and numerically summarized in Table 5. In this comparison one has to bear in mind the size of the data sample. There was 91 matchup pair in the nighttime case, and 102 in the daytime, primarily concentrated in the summer period (50 and 62 pairs, respectively).

The Figure 6 presents the patterns of residual temperature variability. More specifically, Figure 6a shows "empirically the best" solution obtained by fitting the satellite brightness temperatures to the bulk temperatures from Ivana-A, using all the matchup pairs described in the data section. It provides zero-bias, minimum-scatter solution, suggesting attainable error metric as limited by the algorithm form and data quality, and offering a good reference for other solutions. The existence of the patterns even in this solution testifies to the fact that not exactly the same SST value is registered below the surface and at the TOA, either at nighttime or at daytime. Imperfect cloud masking or residual stratification may have contributed to the error in residuals, but diurnal warming appears to be the prime contributor

to the daytime residual. The global coefficient solution (Figure 6b) on the other hand is an example of a “routine application” of the SST algorithms. The solution exhibits much larger scatter, less symmetrical around zero in daytime case, therefore producing a significant bias. Both of these solutions provide bulk SST estimate, making it legitimate to compare them directly to the Ivana-A measurements (1m depth). The comparison metric is listed in Table 5. For the data-fit case, the table shows expected zero bias for both nighttime and daytime, with the scatter of 0.33 and 0.66 respectively. One notes about twice larger mad and rmsd values in daytime estimates, primarily due to diurnal warming effect (not addressed in the study). Global-coefficient solutions exhibit the largest scatter with smallest bias during night and largest bias during day; large mad values (0.43, 0.68) suggest considerable discrepancy throughout the year. Closer inspection of the Figure 6b reveals that the nighttime bias is small due to mutual balancing of positive (primarily in warmer part of the year) and negative (primarily in colder part of the year) SST residuals.

Our two ERA40-based solutions (Figures 6c and 6d) provide remarkably similar residual patterns that also show persistent positive bias. The similarity implies that the regional and seasonal water-vapour effect can be accounted for with equal success by either using “classical” split-window coefficients seasonally adjusted to local climatology (four sets of coefficients), or by explicitly accommodating the water vapour dependence, relying on its own climatology as well as on the tcwv values for the year in question (2004). The plots in Figure 6e (the difference between the Figure 6d and Figure 6c residuals) reinforce that conclusion for both nighttime and daytime.

As pointed out earlier, our ERA40-based solutions provide skin SST estimates which are not directly comparable with the Ivana-A measurements. Skin-to-subskin model would usually suffice in the nighttime case, but daytime solution further requires diurnal heating modelling, if one is interested in bulk solution. These corrections are still subject to active

research. For example, using almost 6000 skin and bulk temperature measurements collected over four-year period Murray et al (2000) found the mean skin-bulk SST difference of $-0.2 \pm 0.46\text{K}$ at night, and $+0.05 \pm 0.51\text{K}$ during daytime; for the low wind conditions (prevailing in summer months over the Adriatic Sea) Murray et al found the mean skin-bulk daytime difference of approximately 0.8 K. On the other hand, Donlon and Robinson (1998) report less than 0.05K in situ skin-bulk temperature difference ascribing it to the high wind speeds that dominate their dataset. In an effort to avoid introduction of two more still researched models, which themselves require additional data and introduce their own uncertainties, we have kept the ERA40 solutions uncorrected, and focused more on the scatter in residuals. One notes in Table 5 that all ERA40 based solutions exhibit a positive bias, in line with Merchant and LeBorgne (2004) finding that “SSTs from RT-based coefficients are likely to be biased by up to several tenths of a kelvin”. An extra step is thus required for empirical adjustment of the offset in our ERA40 derived algorithms, based on additional accurate and representative validation data. It is worth noting here that such an offset correction could also include “the adjustment to the bulk framework”, if appropriate information is available (Merchant and LeBorgne, 2004). Regardless of the bias/offset issue, the RT-based solutions provide standard deviation much better than the global ones, numerically very close to the data-fit reference values. The same level of scatter is attained with either seasonal or tcwv-dependent coefficients. Data paucity notwithstanding, the scatter exhibits seasonal variability (not listed). The Adriatic_seasonal winter solution provides the lowest (std=0.26) and the Adriatic_water_vapor summer solution the highest (std=0.70) value.

Concluding remarks

The aim of this work has been exploration of the regional atmospheric influence on satellite estimation of the Adriatic SST. To that end an ECMWF ERA-40 reanalysis subset

was employed to provide the temperature and humidity profiles as well as surface data, whereas the RTTOV 8.7 radiative transfer model was used to calculate the top of atmosphere brightness temperatures in the AVHRR channels. Ten ERA-40 grid points over the Adriatic Sea were used in the analysis, providing 29590 clear-sky (00 UTC and 12 UTC) profiles, employed in the RT model to calculate respective BTs. The BTs were subsequently fit to the same SST series in order to derive regression coefficients that capture local atmospheric influence.

Climatological analysis of the ERA-40 temperature and specific humidity profiles demonstrated distinct seasonal variability in the ECMWF-modelled atmosphere over the Adriatic. Derived Adriatic average summer vertical temperature distribution proved to be similar to its mid-latitude counterpart, whereas the average ECMWF winter profile exhibited almost 10 K higher values in the lower troposphere. The average Adriatic summer humidity profile has revealed values consistently higher than the mid-latitude profile, while the winter Adriatic and mid-latitude profiles have shown much closer agreement, except above the 900 hPa level. Seasonality noted in temperature and specific humidity profiles also evinced in atmospheric transmittance, thermal channels temperature deficit, and derived parameters like ρ and γ .

To explore the influence of the ERA-40 inferred atmospheric variability on the SST estimates ten coefficient sets were generated using multivariate analysis. Derived Adriatic coefficients exhibited smaller noise amplification than the global ones, also displaying consistent seasonal differences. The SST estimates based on the derived coefficients were compared to an eleven-month long series of SST measurements taken at a station in the northern Adriatic Sea. A least-square fit to this data set was also done, for reference, predictably providing the lowest bias and the smallest scatter. The application of global coefficients produced the largest scatter. Recognition of the local atmospheric conditions

primarily reduced the noise amplification of the instrumental uncertainties in the channel brightness temperatures and consequently lowered the scatter (improved precision) of the SST estimates, as evidenced by three different metrics (standard deviation, mean absolute difference, and root mean square difference). The ERA40-derived solutions generated bias known to appear in RTM-coefficient solutions, requiring further adjustment. Almost identical SST residual obtained using seasonally adjusted “classical” split-window coefficients and by explicitly accommodating water vapour dependence strengthens the credibility of regional coefficients. It further reinforces the notion that the over-the-Adriatic atmosphere may exhibit variability which globally adjusted correction can not fully accommodate.

Although at least one more step (offset adjustment) is needed before obtained coefficients that can be considered as replacement of the operational ones, they are already demonstrating the impact that acknowledging local over-the-Adriatic atmospheric conditions may have on the SST estimates. We believe that the reported results, although focused on the Adriatic Sea are also relevant for other seas at similar latitudes. They warrant further efforts aimed at deriving the necessary offset adjustment, as well as improving understanding of regional atmospheric influence on the remotely sensed SST. In those efforts one should bear in mind previous findings that the use of more channels (e.g. Deschamps and Phulpin, 1980) or more atmospheric information (e.g. Schluessel et al, 1987) both have the potential to improve the SST estimates, but also acknowledging more general limitations (Merchant et al, 2006).

Acknowledgements

This work has been supported by the Croatian Ministry of Science, Education and Sports through the research grant 098-0982705-2707 and via Project Jadran. The ECMWF kindly allowed access to their ERA-40 data. Dr. John Sapper provided the NOAA/NESDIS

global coefficients. Authors are grateful to INAgip and Croatian Hydrographical Institute for making available the SST data collected at the Ivana-A platform. Two reviewers provided constructive and insightful comments that greatly improved the manuscript.

References

- Anding D and Kauth R (1970) Estimation of sea surface from space. *Remote Sense Environ* 1: 217 – 220
- Arbelo M, Hernandez-Leal P, Diaz J P, Exposito F J and Herrera F (2000) Efficiency of a global algorithm for retrieving SST from satellite data in a subtropical region. *Adv Space Res* 25: 1041-1044
- Beljaars A C M (1998) Air-sea interaction in the ECMWF model. Seminar on atmosphere-surface interaction, 8-12 September 1997, 33 – 52
- Bordes P, Brunel P and Marsouin A (1992) Automatic Adjustment of AVHRR Navigation. *J Atmos Ocean Technol* 9: 15-27
- Brunel P and Marsouin A (2000) Operational AVHRR navigation results. *Inter J Remote Sensing* 21: 951-972
- Chevallier F (2001) Sampled databases of 60-level atmospheric profiles from the ECMWF analyses. EUMETSAT/ECMWF SAF Programme Research Report No 4, 27 pp
- Dechamps PY and Phulpin T (1980) Atmospheric correction of infrared measurements of sea surface temperature using channels at 3.7, 11 and 12 μm . *Boundary-Layer Meteor* 18: 131- 143
- Donlon CJ and Robinson IS (1998) Radiometric validation of ETS-1 Along-Track Scanning radiometer average sea surface temperature in the Atlantic Ocean. *J Atmos Ocean Technol* 15:647-660
- Donlon CJ, Minnett PJ, Gentemann C, Nightingale TJ, Barton IJ, Ward B, and Murray MJ (2002) Toward improved validation of satellite sea surface skin temperature measurements for climate research. *J Climate*, 15: 353 - 369
- Eugenio F, Marcello J, Hernandez-Guerra A, and Rovaris E (2005) Regional optimization of an atmospheric correction algorithm for the retrieval of sea surface temperature from

- the Canary Islands –Azores- Gibraltar area using NOAA/AVHRR data. *Int J Remote Sensing* 26: 1799-1814
- Eyre JR (1987) On systematic errors in satellite sounding products and their climatological mean values. *Q J R Meteorol Soc* 113: 279 – 292
- Eyre JR and Woolf HM (1998) Transmittance of atmospheric gases in the microwave region: a fast model. *Appl Optics* 27: 3244-3249
- Eyre JR (1991) A fast radiative transfer model for satellite sounding systems. ECMWF Research Dept Tech Memo 176, ECMWF, 28 pp
- Eyre JR and Woolf HM (1988) Transmittance of atmospheric gases in the microwave region: a fast model. *Appl Optics* 27: 3244-3249
- Kent EC, Forrester TN, and Taylor PK (1996) A comparison of oceanic skin effect parameterizations using shipborne radiometer data. *J Geophys Res* 101 (C7): 16649 - 16666
- Kilpatrick KA, Podesta GP and Evans R (2001) Overview of the NOAA/NASA advanced very high resolution radiometer Pathfinder algorithm for sea surface temperature and associated matchup data base. *J Geophys Res* 106 (C5): 9179-9197.
- Klaes D (1997) The EUMETSAT ATOVS and AVHRR processing package (AAPP). Proceedings of the 1997 Meteorological Satellite Data Users' Conference, Brussels, Belgium, 29 September – 3 October 1997, Proceedings EUM P 21
- Kleespies TJ and McMillin LM (1990) Retrieval of precipitable water from observations in the split window over varying surface temperatures. *J Appl Meteorol* 29: 851 - 862
- Masuda K, Takashima T and Takayama Y (1988) Emissivity of pure and sea waters for the model sea surface in the infrared window region. *Remote Sense Environ* 24: 313-329
- McMillin LM (1975) Estimation of sea surface temperatures from two infrared window measurements with different absorption. *J Geophys Res* 80:5113-5117

- McMillin LM and Fleming HE (1976) Atmospheric transmittance of an absorbing gas: A computationally fast and accurate transmittance model for absorbing gases with constant mixing ratios in inhomogeneous atmospheres. *App Optics* 15: 358–363
- Merchant CJ, Filipiak MJ, LeBorgne P, Roquet H, Autret E, Piolle J-F, and Lavender S (2008) Diurnal warm-layer events in the western Mediterranean and European shelf seas. *Geophys Res Lett* 35, doi: 10.1029/2007GL033071
- Merchant CJ and Le Borge P (2004) Retrieval of sea surface temperature from space, based on modelling of infrared radiative transfer: Capabilities and limitations. *J Atmos Oceanic Tech* 21: 1734-1746
- Merchant C J, Horrocks L A, Eyre J R, and O'Carroll A G (2006) Retrievals of sea surface temperature from infrared imagery: origin and form of systematic errors. *Q J R Meteorol Soc* 132:1205 - 1223
- Minnett PJ (1986) A numerical study of the effects of anomalous North Atlantic atmospheric conditions on the infrared measurements of sea surface temperature from space. *J Geophys Res* 91: 8509 - 8521
- Minnett PJ (1990) The regional optimization of infrared measurements of sea surface temperature. *J Geophys Res* 95: 13,497-13,510
- Murray MJ, Allen MR, Merchant CJ, Harris AR, and CJ Donlon 2000 Direct observations of skin-bulk variability. *Geophys Res Lett* 27: 1171-1174
- O'Carroll AG, Watts J G, Horrocks LA Saunders RW, and Rayner NA 2006 Validation of the AATSR meteo product sea surface temperature. *J Atmos Oceanic Tech* 23: 711-726
- Pearce AF, Prata A J, Manning CR (1989) Comparison of NOAA/AVHRR-2 sea surface temperature with surface measurements in coastal waters *Inter J Remote Sensing* 10: 37-52

- Persson A and Grazzini (2007) User Guide to ECMWF forecast products. Meteorological Bulletin M3.2, ECMWF, 161 pp
- Rayer PJ (1995) Fast transmittance model for satellite sounding. *Appl Optics* 34: 7387- 7394
- Saunders R, Matricardi M, Brunel P (1999) An improved fast radiative transfer model for assimilation of satellite radiance observations. *Quart J Roy Met Soc* 125: 1407-1425
- Saunders R and Brunel P (2005) RTTOV_8_7 Users Guide. EUMETSAT NWP SAF, NWPSAF-MO-UD-008, 45 pp
- Saunders R with Contributors (2005) RTTOV-8 science and validation report. NWPSAF-MO-TV-007, 46 pp
- Schluessel P, Shin H-Y, Emery WJ, and Grassl H 1987 Comparison of satellite-derived sea surface temperatures with in situ skin measurements. *J Geophys Res* 92: 2859-2874
- Shenoi SC (1999) On the suitability of global algorithms for the retrieval of SST from the north Indian Ocean using NOAA/AVHRR data. *Int J Remote Sens*, 20: 11-29
- Sherlock V (1999) ISEM-6: Infrared surface emissivity model for RTTOV-6. NWP SAF Report. 16 pp
- Strong AE and McClain EP (1984) Improved ocean temperatures from space – comparison with drifting buoys. *Bull Am Meteorol Soc*, 65: 138 - 142
- Tanre D, Holben BN, Kaufman Y (1992) Atmospheric correction algorithm for NOAA-AVHRR products: theory and application. *IEEE Trans Geosci Remote Sensing*, 30 : 231- 248
- Trishchenko AP, Fedosejeva G, Li Z, and Cihlar J (2002) Trends and uncertainties in thermal calibration onboard NOAA-9 to NOAA-16. *J Geophys Res* 107D, doi:10.1029/2002JD002353
- Tomažić I (2006) Validation of remotely sensed Adriatic Sea surface temperature. MSc Thesis, University of Zagreb, 170 pp

Uppala SM and 45 Co-Authors (2005) The ERA-40 re-analysis. *Quart J R Meteorol Soc*, 131: 2961-3012

Zavody AM, Mutlow CT and Llewellyn-Jones DT (1995) A radiative transfer model for sea surface temperature retrieval for the along-track scanning radiometer. *J Geophys Res* 100: 937-952

Zhang H-M, Reynolds RW, and Smith TM (2004) Bias characteristics in the AVHRR sea surface temperature. *Geophys Res Lett* 31, L01307, doi: 10.1029/2003GL018804

Corresponding author's address:

Dr. Milivoj Kuzmić, Ruđer Bošković Institute, Center for Marine and Environmental Research, Bijenička cesta 54, HR-10002 Zagreb, Croatia (e-mail: kuzmic@irb.hr)

Table 1. Seasonal and geographic distribution of clear-sky ERA-40 profiles included in the analysis.

Adriatic	North		Middle		South		Whole		
	Day	Night	Day	Night	Day	Night	Day	Night	Total
Q1	273	358	509	449	925	960	1707	1767	3474
Q2	470	824	859	1258	1243	2257	2572	4339	6911
Q3	1109	1708	2041	2822	3231	5088	6381	9618	15999
Q4	205	196	414	427	974	990	1593	1613	3206
ALL	2057	3086	3823	4956	6373	9295	12253	17337	29590

Table 2 Seasonal distribution of average temperature (T) and specific humidity (q) in the upper (U) and lower (L) atmosphere. Temperatures are in Kelvins, specific humidities in kg/kg. Also listed are values for the mid-latitude winter, mid-latitude summer and US Standard atmospheres.

	T_U	T_L	q_U	q_L
Q1 Winter	240.760	279.409	0.0004	0.0028
Q2 Spring	246.516	290.103	0.0009	0.0059
Q3 Summer	250.143	294.817	0.0011	0.0077
Q4 Autumn	244.076	284.184	0.0006	0.0045
Annual	247.537	290.755	0.0009	0.0064
Mid Lat Winter	239.353	270.202	0.0005	0.0024
Mid Lat Summer	251.268	291.586	0.0015	0.0098
US standard	243.464	284.539	0.0008	0.0042

Table 3 Seasonal and geographical variability of channel temperature deficit, ρ parameter and γ parameter values derived for the AVHRR sensor on NOAA16 platform.

Channel Temperature Deficit				
	$T_4 - T_s$		$T_5 - T_s$	
	Day	Night	Day	Night
Winter	-1.267	-1.245	-1.920	-1.881
Spring	-1.510	-1.610	-2.306	-2.453
Summer	-2.028	-2.103	-3.098	-3.202
Autumn	-1.694	-1.719	-2.581	-2.614
Average	-1.770	-1.857	-2.700	-2.825

	ρ							
Adriatic	North		Middle		South		Whole	
	Day	Night	Day	Night	Day	Night	Day	Night
Winter	0.951	0.947	0.948	0.944	0.948	0.945	0.948	0.945
Spring	0.905	0.891	0.900	0.889	0.898	0.886	0.900	0.888
Summer	0.869	0.854	0.868	0.857	0.870	0.858	0.869	0.857
Autumn	0.929	0.918	0.923	0.914	0.920	0.915	0.922	0.915
Average								

	γ							
Adriatic	North		Middle		South		Whole	
	Day	Night	Day	Night	Day	Night	Day	Night
Winter	1.630	1.646	1.638	1.664	1.646	1.660	1.641	1.658
Spring	1.912	2.022	1.951	2.033	1.965	2.053	1.951	2.041
Summer	2.179	2.292	2.188	2.270	2.169	2.261	2.177	2.269
Autumn	1.758	1.838	1.802	1.858	1.821	1.851	1.808	1.851
Average	1.870	1.950	1.895	1.956	1.900	1.956	1.894	1.955

Table 4. The split-window SST algorithm coefficients (equation 7) calculated acknowledging over-the-Adriatic conditions derived from the ERA-40 data. A constant value of 273.15 is subtracted from all a_0 values. Also listed are the NAF (equation 8), and global coefficient values. NAF is calculated for nadir view.

	a_0	a_1	a_2	NAF	a_3	$a_4 10^{-3}$	$a_5 10^{-5}$
Daytime							
Global	0.91400	0.99975	2.39418	4.15342	0.73235		
Adriatic winter	2.09690	1.00875	1.33388	2.69578	0.72375		
Adriatic spring	-0.91123	0.99724	1.74531	3.25079	0.58759		
Adriatic summer	-4.83591	0.98349	1.91473	3.47360	0.54306		
Adriatic autumn	4.52428	1.01643	1.64507	3.12887	0.63682		
Adriatic w. vap	-0.65025	1.00248	1.87548	3.43513	0.57931	4.67300	5.20000
Nighttime							
Global	-0.29200	0.99439	2.55546	4.37399	0.71418		
Adriatic winter	2.77334	1.01097	1.41862	2.81344	0.69785		
Adriatic spring	-1.89957	0.99344	1.89297	3.45177	0.53830		
Adriatic summer	-7.77068	0.97323	1.99571	3.57735	0.50638		
Adriatic autumn	4.39675	1.01589	1.69325	3.19477	0.63096		
Adriatic w. vap	-0.45005	0.99843	1.99292	3.59443	0.54402	5.64600	6.70000

Table 5 Statistical measures (in °C) for the SST residuals plotted in Figure 6a and 6b. Bias, standard deviation (std), mean absolute difference (mad), and root mean square difference (rmsd) values are listed, separately for daytime and nighttime.

Coefficient set	Night				Day			
	bias	std	mad	rmsd	bias	std	mad	rmsd
Fit to Ivana data	0.00	0.33	0.28	0.33	0.00	0.66	0.45	0.60
Global	-0.04	0.55	0.43	0.55	0.46	0.73	0.68	0.86
Adriatic_seasonal	0.16	0.36	0.32	0.40	0.40	0.66	0.59	0.77
Adriatic_water_vapor	0.20	0.36	0.33	0.41	0.40	0.67	0.59	0.78
water_vapor - seasonal	0.04	0.01	0.01	0.01	0.01	0.09	0.00	0.01

Figure captions

Figure 1. Location of the ERA-40 grid-points over the Adriatic Sea. Also marked are the locations of the INAgip Ivana-A station, the cities of Rovinj and Korčula, as well as the northern, middle and southern Adriatic boundaries.

Figure 2. a)- d) Comparison of the ERA-40 derived mean vertical profile of temperature for the entire Adriatic Sea (thin line) with the mean vertical profiles for different seasons (Q1-Q4, thick line); e) ERA-40 seasonal with mid-latitude winter and mid-latitude summer profiles, and f) ERA-40 derived mean with US standard atmosphere mean profile, at the RTTOV model pressure levels.; g) Annual cycle of 2m ERA-40 derived temperature with respective data for two coastal stations and the 1981-1995 period. Horizontal bars have the length of double standard deviation and are centred at the mean.

Figure 3. a)- d) Comparison of the ERA-40 derived mean vertical profile of specific humidity for the entire Adriatic Sea (thin line) with the mean vertical profiles for different seasons (Q1-Q4, thick line); e) ERA-40 seasonal with mid-latitude winter and mid-latitude summer profiles, and f) ERA-40 derived mean with US standard atmosphere mean profile, at the RTTOV model pressure levels. Horizontal bars have the length of double standard deviation and are centred at the mean.

Figure 4. The annual cycle of monthly anomaly of a) specific humidity anomaly in the upper atmosphere (above 850 hPa); b) temperature anomaly of the lower troposphere; c) total

column water vapour; d) temperature difference at the air-sea interface; and e) number of data points. Separate daytime and nighttime curves are plotted.

Figure 5. Monthly scatter plots of ERA40 total column water vapour against thermal channels temperature difference derived from RTM calculations. All Adriatic points are combined.

Figure 6. Nighttime and daytime sea surface temperature residuals (satellite-in situ) calculated with a) fit to Ivana-A; b) global; c) Adriatic seasonal; and d) Adriatic water vapour dependent set of coefficients. e) Difference between d) and c) residual.

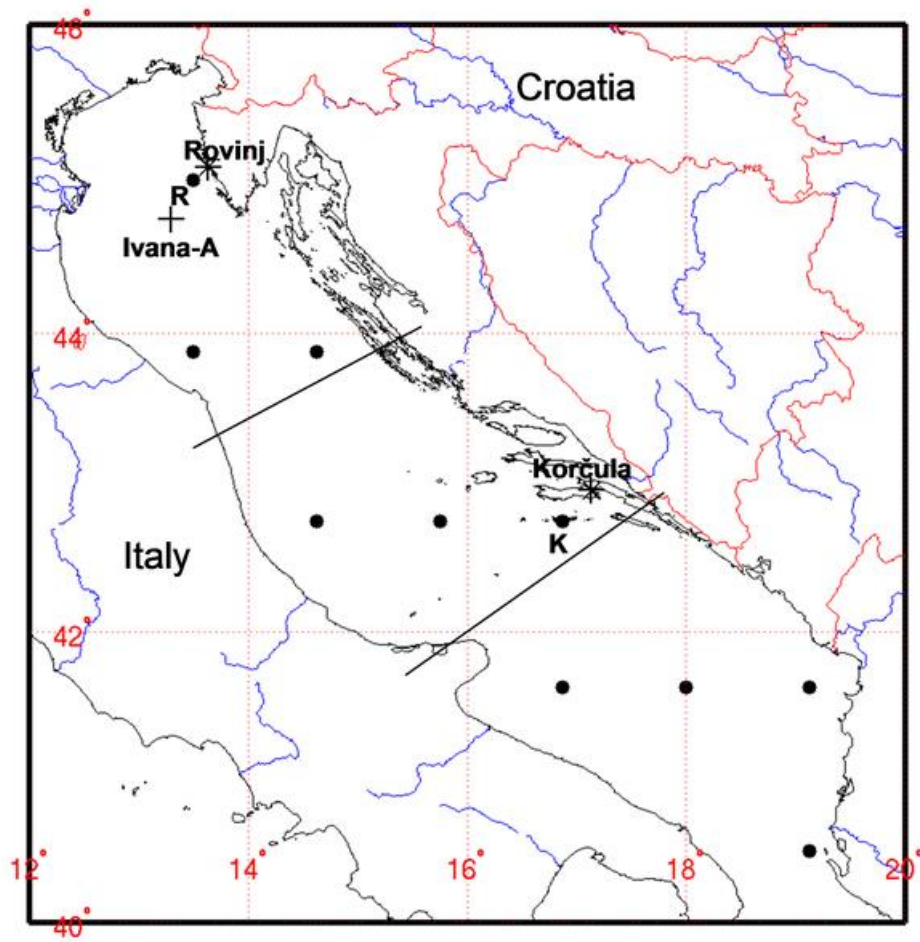


Figure 1.

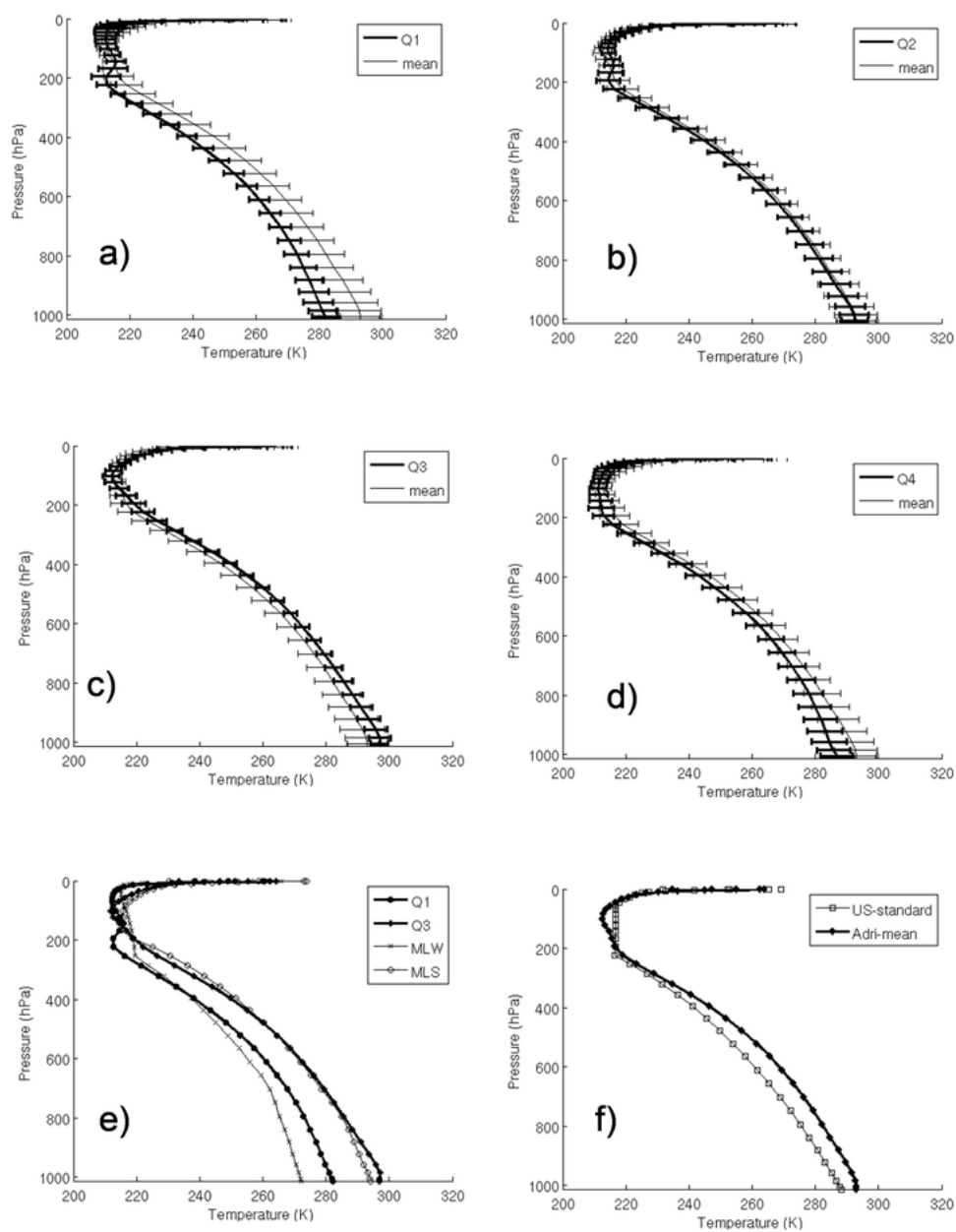


Figure 2

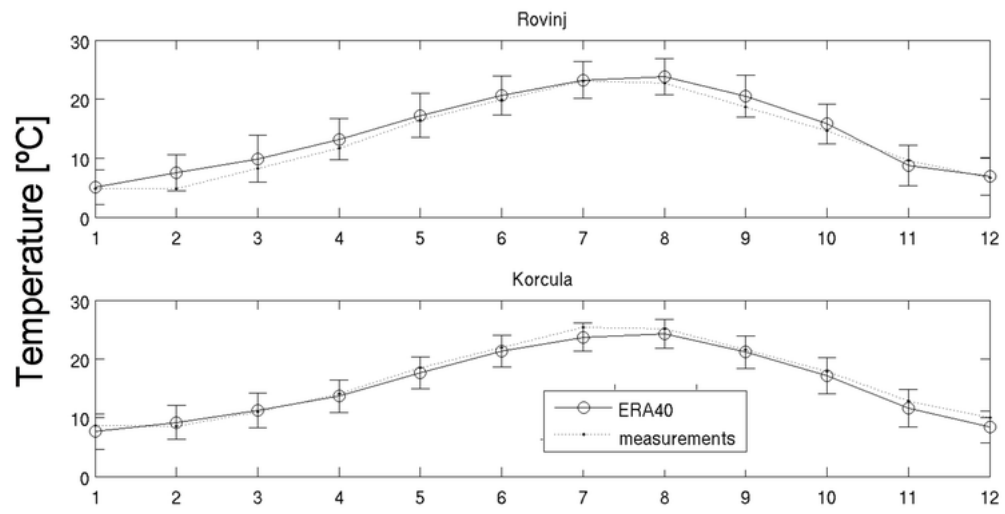


Figure 2g

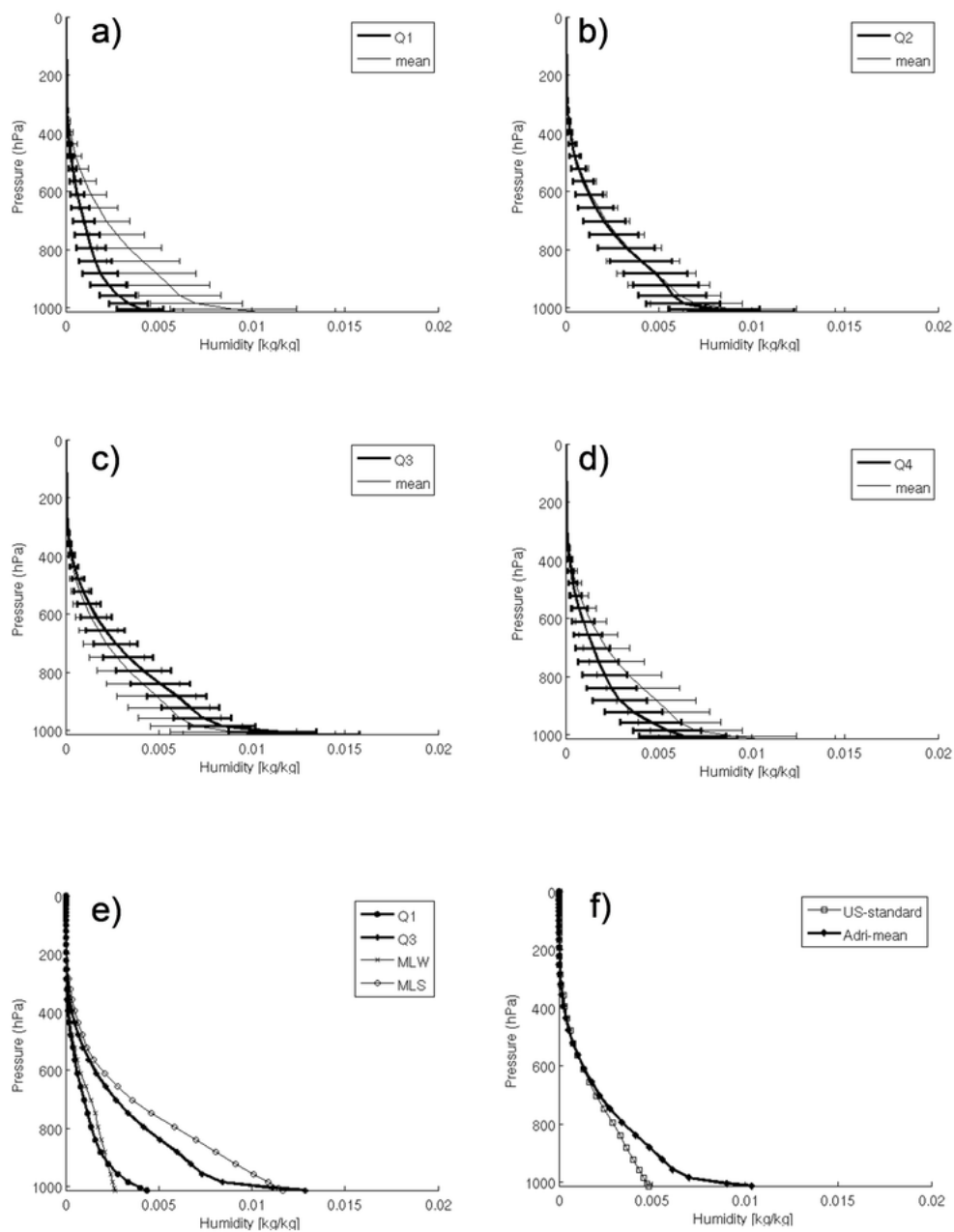


Figure 3.

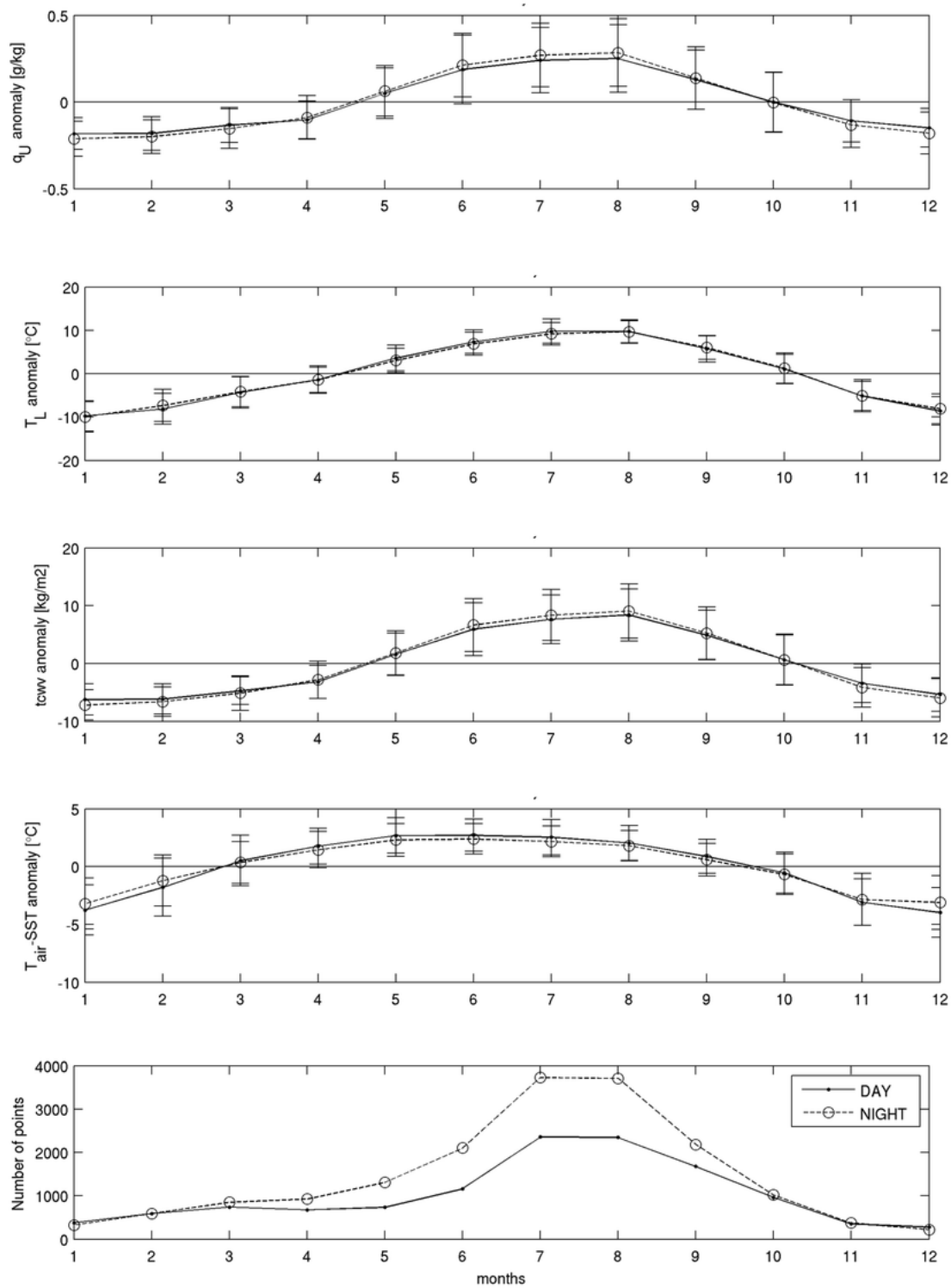


Figure 4.

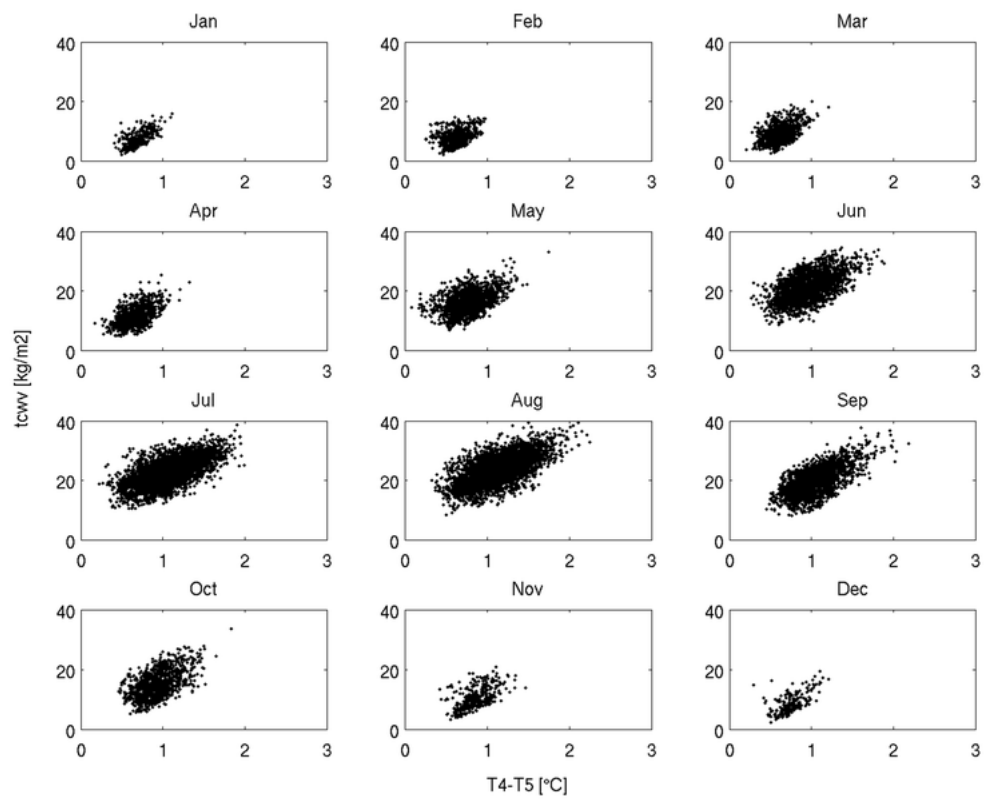


Figure 5

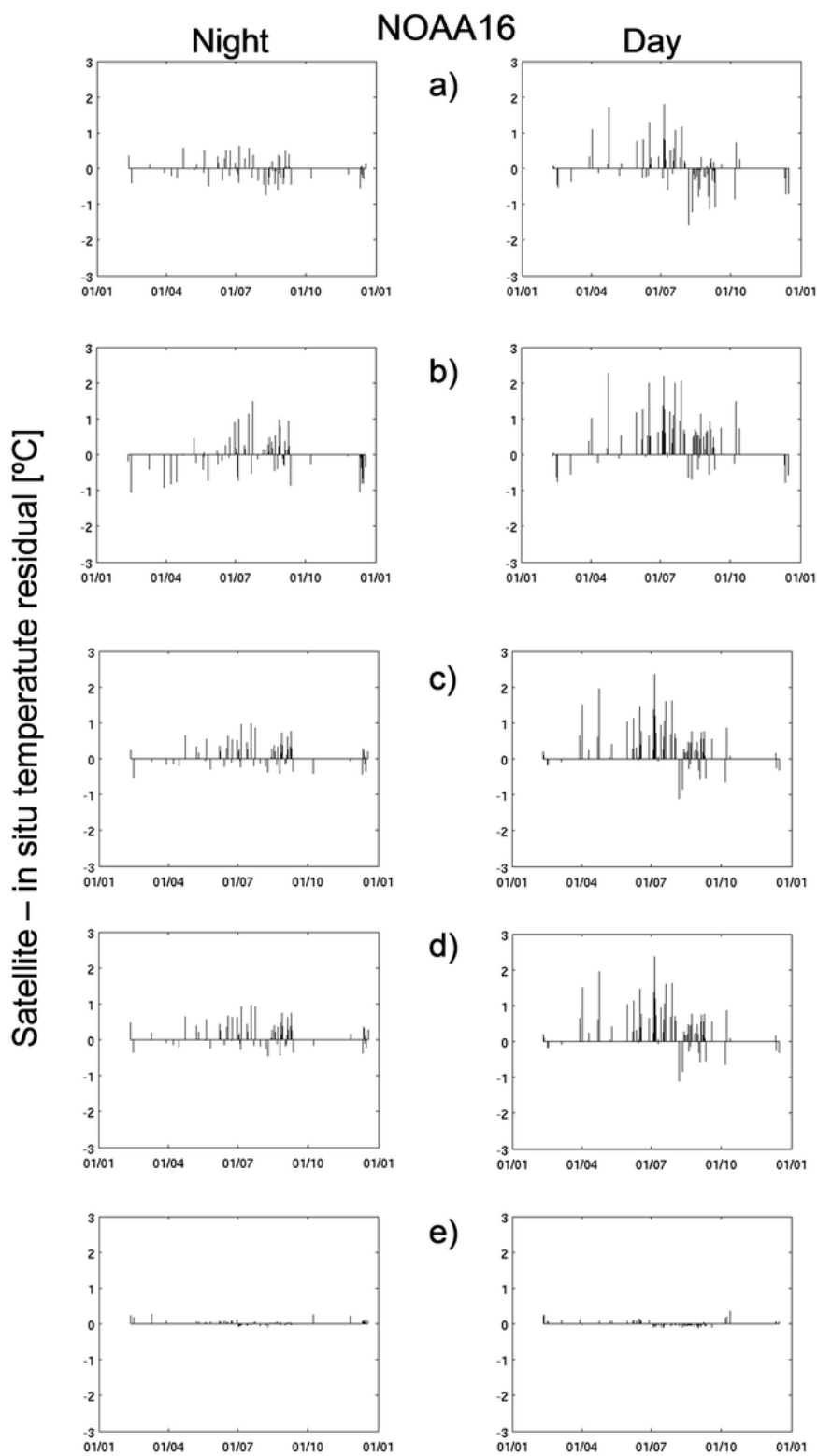


Figure 6